Supporting Informatin

3D Ln^{III}-MOFs: slow magnetic relaxation and highly sensitive luminescent detection of Fe^{3+} and ketones

Fei Zhao, Xiao-Yu Guo, Zhen-Peng Dong, Zhi-Liang Liu and Yan-Qin Wang*

Table S1. The selected bond lengths (Å) and angles (◦) for Eu-MOF(**4**).

Eu1-O2A	2.328(9)	Eu1-O6C	2.379(8)
Eu1-O8A	2.331(9)	Eu1-O5B	2.388(8)
Eu1-O1	2.393(9)	Eu1-O7	2.422(9)
Eu1-O10	2.451(13)	Eu1-O9	2.551(11)
O2A-Eu1-O8A	73.0(3)	O2A-Eu1-O6C	147.6(4)
O8A-Eu1-O6C	137.9(3)	O2A-Eu1-O5B	84.2(3)
O8A-Eu1-O5B	81.7(3)	O6C-Eu1-O5B	90.7(3)
O2A-Eu1-O1	121.4(3)	O8A-Eu1-O1	78.2(3)
O6C-Eu1-O1	81.9(3)	O5B-Eu1-O1	139.9(3)
O2A-Eu1-O7	80.4(3)	O8A-Eu1-O7	121.7(3)
O6C-Eu1-O7	86.4(3)	O5B-Eu1-O7	145.9(4)
O1-Eu1-O7	73.2(3)	O2A-Eu1-O10	76.9(4)
O8A-Eu1-O10	143.0(4)	O6C-Eu1-O10	70.9(4)
O5B-Eu1-O10	74.2(4)	O1-Eu1-O10	137.3(4)
O7-Eu1-O10	72.8(4)	O2A-Eu1-O9	137.0(3)
O8A-Eu1-O9	69.2(3)	O6C-Eu1-O9	69.2(4)
O5B-Eu1-O9	70.7(3)	O1-Eu1-O9	69.8(3)
O7-Eu1-O9	137.9(3)	O10-Eu1-O9	125.4(4)

Symmetry transformations used to generate equivalent atoms: A: -x+1,-y+1,-z+1; B: -x+2,-y+1,-z; C: x,y,z+1.

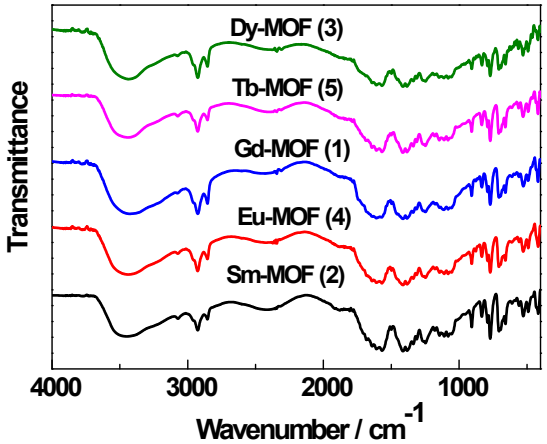

Fig. S1 The IR spectra of five LnMOFs.

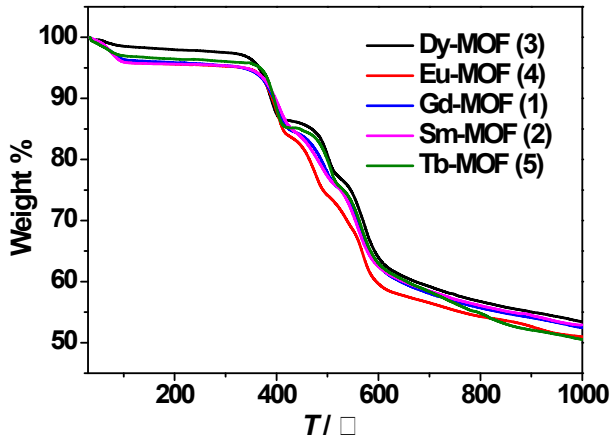

Fig. S2 The TGA curve for Ln-MOFs**.**

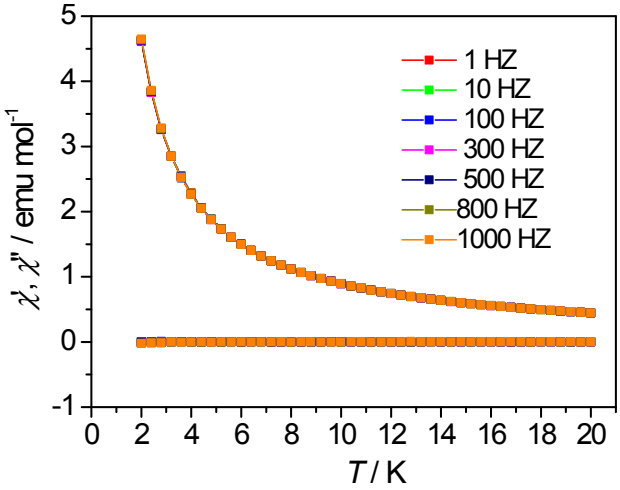

Fig. S3 Frequency dependence of the ac susceptibility for Gd-MOF(**1**) under zero dc field at 1, 10, 100, 300, 500, 800 and 1000 Hz.

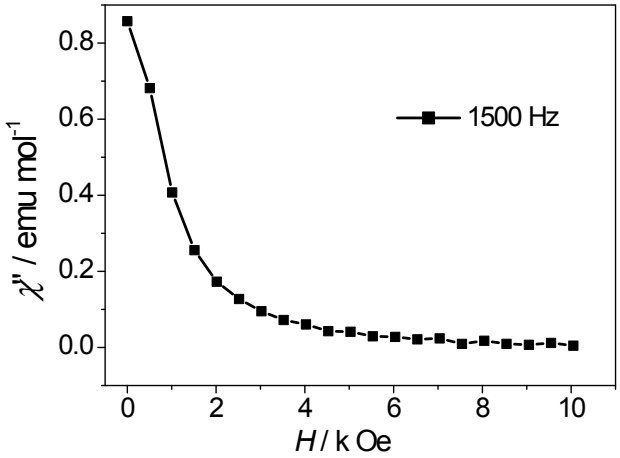

Fig. S4 The out-of-phase (χ'') ac susceptibility for Dy-MOF(**3**) (2 K, f = 1500 Hz) under the applied static field from 0-10 kOe.

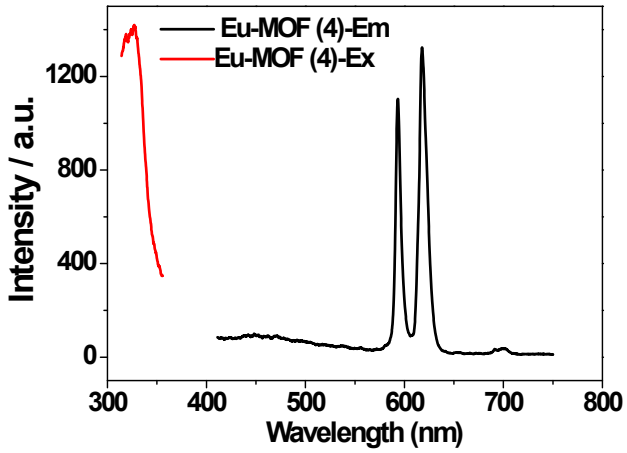

Fig. S5 The solid-state excitation and emission spectra of Eu-MOF(**4**) at room temperature.

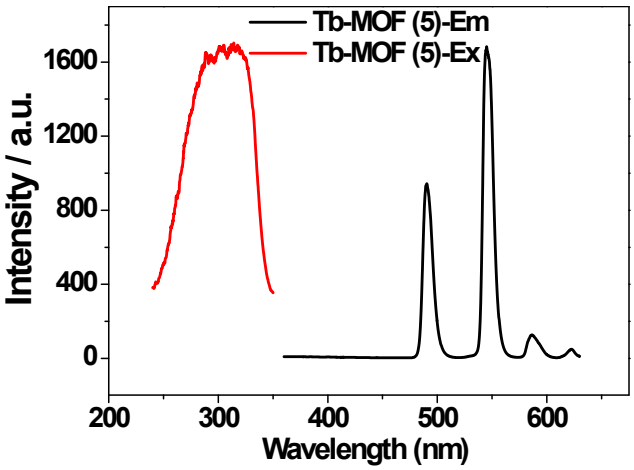

Fig. S6 The solid-state excitation and emission spectra of Tb-MOF(**5**) at room temperature.

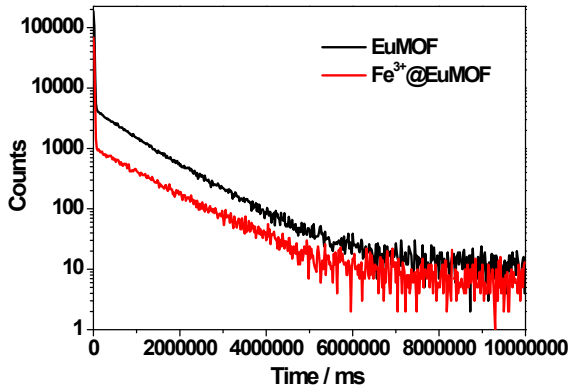

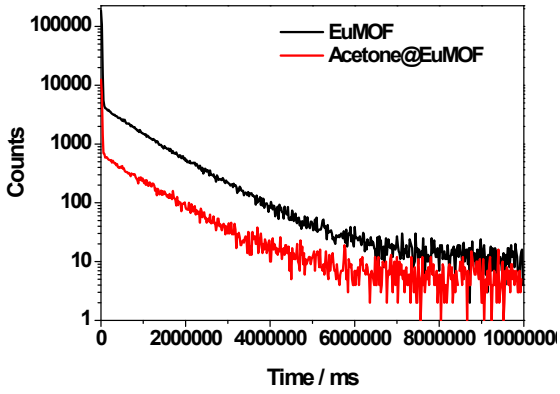

Fig. S7 Semilog plots of fluorescence decay versus time for Eu-MOF(**4**) and Eu-MOF(**4**)@Fe^{3+} (top), and Eu-MOF(**4**)@acetone (bottom).

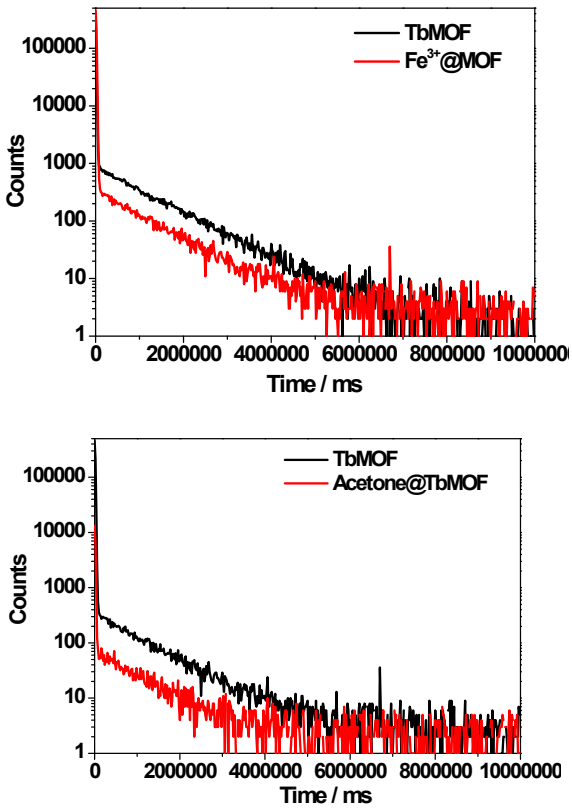

Fig. S8 Semilog plots of fluorescence decay versus time for Tb-MOF(**5**) and Tb -MOF(**5**)@Fe^{3+} (top), and Tb-MOF(**5**)@acetone (bottom).

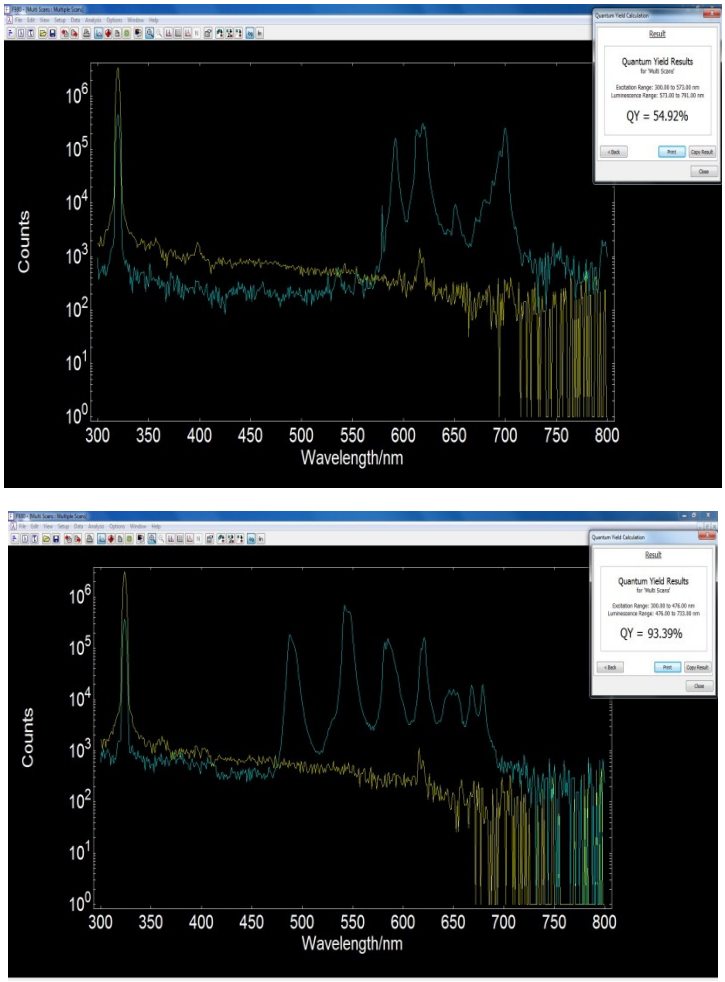

Fig. S9 top: The test data of absolute quantum yield of Eu-MOF(4); bottom: the test data of absolute quantum yield of Tb-MOF(5).

Table S2. A comparison between Ln^{III}-based MOFs luminescent sensors sensing towards Fe^{3+} and acetone

Analyte	MOF	Solution	Detection Limit	K_{sv}	Ref.
Fe^{3+}	$[Tb(L_1)_{1.5}(H_2O)](H_2O)_3$	water	---	---	S1
Fe^{3+}	$[Eu(HL_2)(DMF)(H_2O)_2](H_2O)_3$	water	---	1.52×10^3	S2
Fe^{3+}	$[Tb(HL_2)(DMF)(H_2O)_2](H_2O)_3$	water	50 μM	4.48×10^3	S2
Fe^{3+}	$[H_2NMe_2][Eu(HL_3)]$	water	---	---	S3
Fe^{3+}	$[Eu_2(L_4)_3(DMA)(H_2O)_3](DMA)(H_2O)_{4.5}$	water	---	1.07×10^4	S4
Fe^{3+}	$[Eu(HL_5)_2(NO_3)](H_2O)$	ethanol	0.026 mmol/L	---	S5
Fe^{3+}	$\{\{Me_2NH_2\}[Tb^{III}(L_6)]\cdot 3H_2O\cdot DMF\}_n$	DMF	10^{-2} mol/L	4.7×10^3	S6
Fe^{3+}	$[Tb(TBOT)(H_2O)](H_2O)_4(DMF)(NMP)_{0.5}$	water	0.13 mmol/L	5.51×10^3	S7

Acetone	$\{[Eu(bpda)_{1.5}]H_2O\}_n$	DMF	0.35 vol%	---	S8
Acetone	$[Eu_4(BPT)_4(DMF)_2(H_2O)_8]$	DMF	5 vol%	48.7	S9

H_2L_1 = 2-(2-hydroxy-propionylamino)-terephthalic acid;

H_4L_2=2,8,14,20-tetra-ethyl-6,12,18,24-tetra-methoxy-4,10,16,22-tetra-carboxy-methoxy-calix[4]arene);

H_4L_3 = tetrakis[4-(carboxyphenyl)oxamethyl]methane acid;

H_2L_4 = 9,9-dimethyl-2,7-fluorenedicarboxylic acid;

H_2L_5 = 3-(1*H*-pyrazol-3-yl) benzoic acid;

H_4L_6 = 5-(bis(4-carboxybenzyl)amino)isophthalic acid;

H_3TBOT = (2,4,6-tris[1-(3-carboxylphenoxy)ylmethyl]mesitylene);

BPDA = biphenyl-2,2 -dicarboxylic acid;

H_3BPT=Biphenyl-3,4′,5-tricarboxylate;

NMP = N-methyl-2-pyrrolidone;

DMF = dimethylformamide;

DMA = dimethylacetamide.

Reference

S1 L.-H. Cao, F. Shi, W.-M. Zhang, S.-Q. Zang and T. C. W. Mak, *Chem. Eur. J.*, 2015, **21**, 15705.

S2 S.-T. Zhang, J. Yang, H. Wu, Y.-Y. Liu and J.-F. Ma, *Chem. Eur. J.*, 2015, **21**, 15806.

S3 S. Dang, E. Ma, Z.-M. Sun and H. Zhang, *J. Mater. Chem*., 2012, **22**, 16920.

S4 L. Li, Q. Chen, Z. Niu, X. Zhou, T. Yang and W. Huang, *J. Mater. Chem. C*, 2016, **4**, 1900.

S5 G.-P. Li, G. Liu, Y.-Z. Li, L. Hou, Y.-Y. Wang and Z. Zhu, *Inorg. Chem.*, 2016, **55**, 3952**.**

S6 X. Guo, Y. Li, Q. Peng, Z. Duan, M. Li, M. Shao, X. He, *Polyhedron,* 2017, **133**, 238-244.

S7 M. Chen, W.-M. Xu, J.-Y. Tian, H. Cui, J.-X. Zhang, C.-S. Liu and M. Du, *J. Mater. Chem. C*., 2017, **5**, 2015-2021.

S8 J. Wang, J. Ru Wang, Y. Li, M. Jiang, L. W. Zhang and P. Y. Wu, *New J. Chem*., 2016, 40, 8600.

S9 Z. M Hao, G. C Yang, X. Z. Song, M. Zhu, X. Meng and S. N. Zhao, *J. Mater. Chem. A*, 2014, **2**, 237.

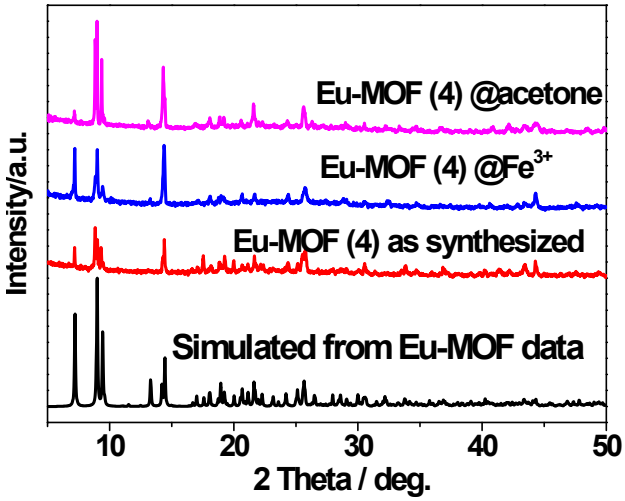

Fig. S10 The PXRD patterns of the as-synthesized Eu-MOF(**4**) after Fe^{3+} and acetone sensing

process, with the simulated result as reference.

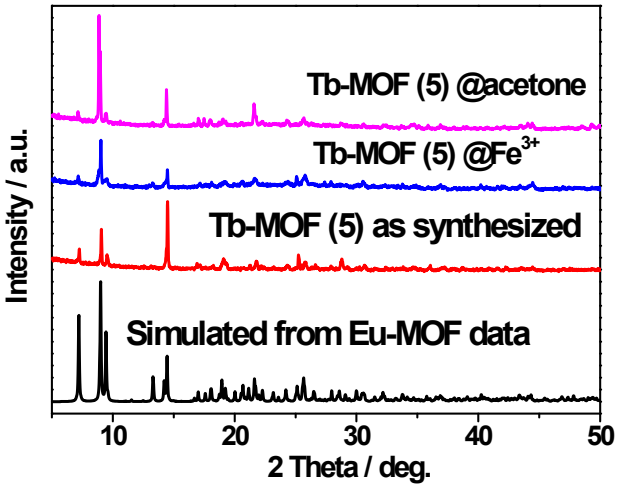

Fig. S11 The PXRD patterns of the as-synthesized Tb-MOF(**5**) after Fe^{3+} and acetone sensing process, with the simulated Eu-MOF(**4**) single crystal data result as reference.

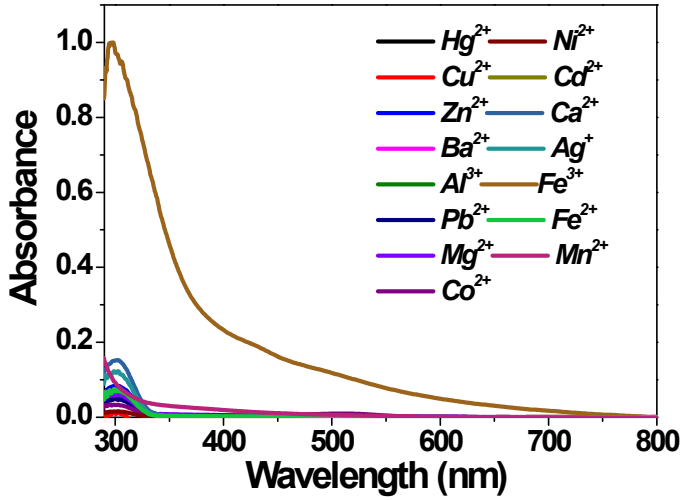

Fig. S12 The UV-Vis absorption spectrum of selected 0.001 M different M^{z+} (Hg^{2+}, Cu^{2+}, Zn^{2+}, Ba^{2+}, Al^{3+}, Pb^{2+}, Mg^{2+}, Co^{2+}, Ag^{+}, Cd^{2+}, Na^{+}, Ca^{2+}, Ni^{2+}, Mn^{2+}, Fe^{2+} and Fe^{3+}) ions aqueous solution.

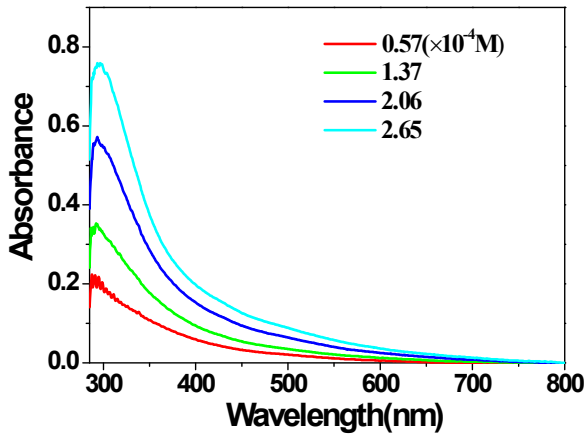

Fig. S13 The UV-Vis absorption spectrum of Eu-MOF(**4**) dispersed in water upon increasing

addition of Fe^{3+} aqueous solution.

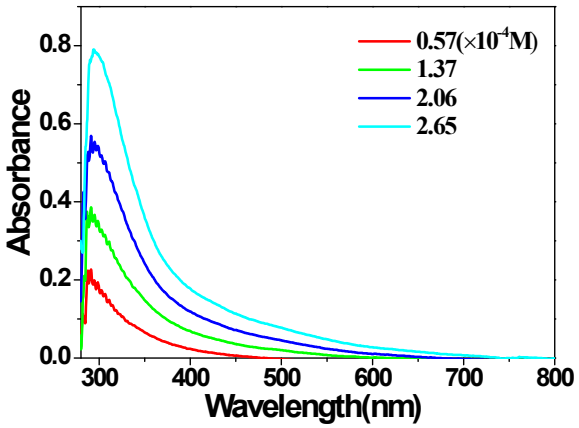

Fig. S14 The UV-Vis absorption spectrum of Tb-MOF(**5**) dispersed in water upon increasing addition of Fe^{3+} aqueous solution.

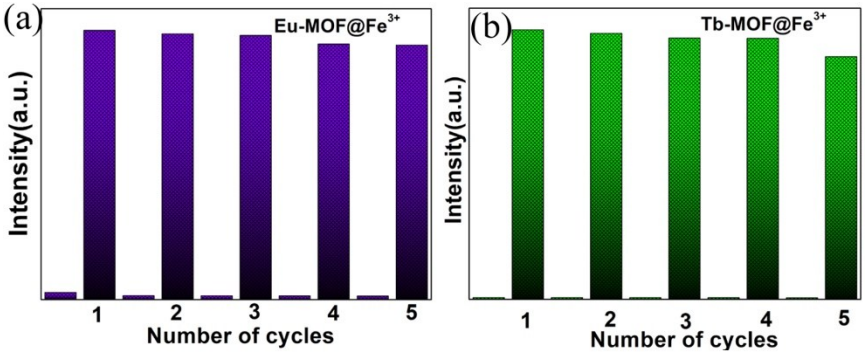

Fig. S15 (a) Five cycle tests of Eu-MOF(**4**) towards sensing Fe^{3+} in simulated biological fluids. (b) Five cycle tests of Tb-MOF(**5**) towards sensing Fe^{3+} in simulated biological fluids.

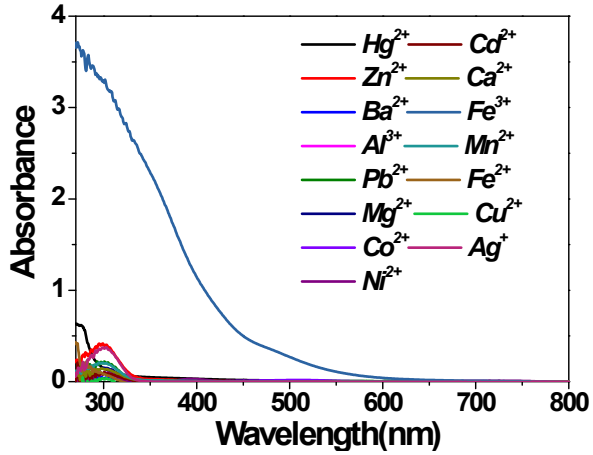

Fig. S16 The UV-Vis absorption spectrum of selected 0.1 M different M^{z+} (Hg^{2+}, Cu^{2+}, Zn^{2+}, Ba^{2+}, Al^{3+}, Pb^{2+}, Mg^{2+}, Co^{2+}, Cd^{2+}, Na^{+}, Ca^{2+}, Ni^{2+}, Mn^{2+}, Fe^{2+} and Fe^{3+}) simulated biological fluids.

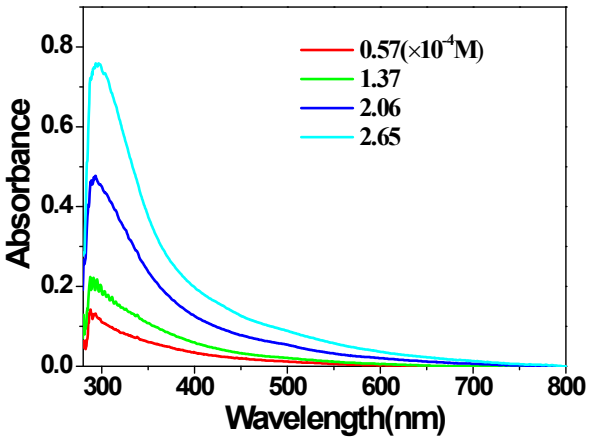

Fig. S17 The UV-Vis absorption spectrum of Eu-MOF(**4**) dispersed in simulated biological fluids upon increasing addition of Fe^{3+} solution.

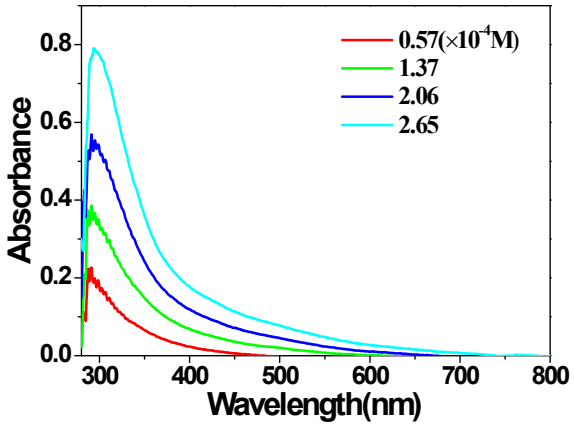

Fig. S18 The UV-Vis absorption spectrum of Tb-MOF(**5**) dispersed in simulated biological fluids upon increasing addition of Fe^{3+} solution.

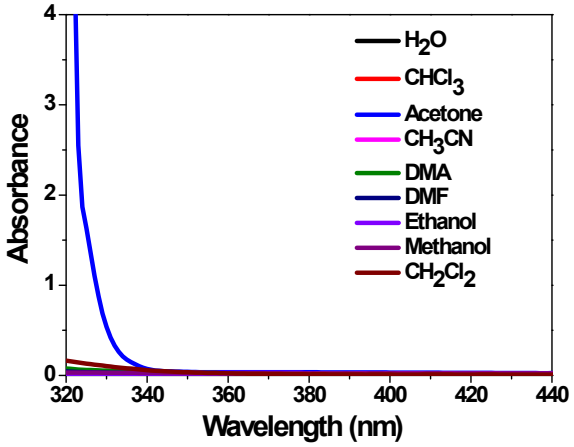

Fig. S19 The UV-Vis absorption spectrum of different small organic solvent molecules in aqueous solution.

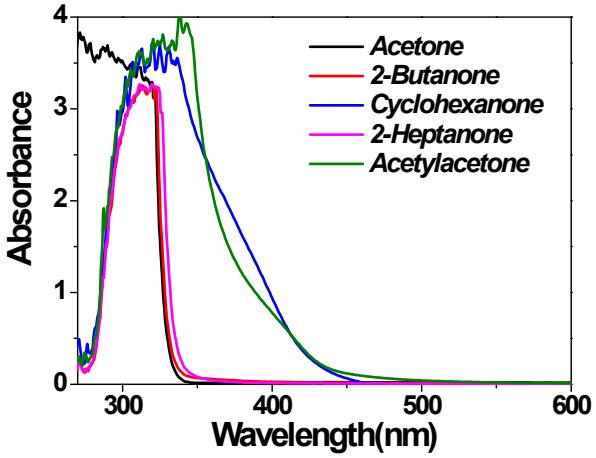

Fig. S20 The UV-Vis absorption spectrum of different laboratory ketones in aqueous solution.